A new method in reservoir rock classification in carbonate and sandstone formations

Hashem Omrani[1], Mastaneh Hajipour[1,*], Saeid Jamshidi[2] and Mohammad Behnood[1]

[1] Department of Petroleum Engineering, Science and Research Branch, Islamic Azad University, Tehran, Hesarak 1477893855, Iran

[2] Department of Chemical and Petroleum Engineering, Sharif University of Technology, Tehran, Azadi avenue 1458889694, Iran

*Corresponding author: Mastaneh Hajipour. E-mail: m.hajipour@srbiau.ac.ir

Abstract

This study aims to improve rock-type classification by analyzing core data based on the water–oil primary drainage capillary pressure method. A modified empirical equation is proposed using permeability, porosity, and irreducible water saturation to classify rock types based on water–oil primary drainage capillary pressure. We used primary drainage capillary pressure data measured in carbonate and sandstone samples in the Ahvaz Asmari and Mansouri oilfields to evaluate the characterization number (Cn) method. This study consists of two main parts. First, the Cn method is introduced to rock typing, and the permeability is calculated from well log data. In the second part, we present rock-type classification when the water saturation of the formation is more than the irreducible water saturation. The novelty of this work is a simple and efficient technique to rock-type classification using the Cn method. In addition, we present a procedure to assign rock types for the transition zone using the Cn method. Moreover, this study systematically investigates the role of irreducible water saturation in rock typing. The innovation of this work lies in its ability to classify rocks in heterogeneous reservoirs for carbonate and sandstone lithology and allow for the calculation of permeability more accurately from well log data. The comparison results between the Cn method and the flow zone indicator method show the robust clustering ability of the Cn method.

Keywords: reservoir rock classification, petrophysical properties, capillary pressure

1. Introduction

Reservoir rock classification is the process of dividing reservoir rocks into separate units with similar properties. Reservoir rock and fluid properties play a critical role in describing the behavior of the reservoir and its complex nature. The differences between capillary pressure curves indicate different pore geometries and rock properties and are depicted by the effect of the rock based on its governing mechanism. In industry, to define rock types, rocks are usually grouped based on their primary drainage capillary pressure (PDCP). In this method, each rock type is a group with similar P_c–S_w curves (Lalanne & Rebelle 2014). In addition, the

PDCP and the corresponding imbibition capillary pressure are usually averaged to create a saturation table for each rock type in reservoir modeling. In this study, rocks with similar primary drainage capillary pressure curves (PDCPCs) are identified and grouped. In dynamic reservoir simulation, the data for each rock type are averaged, and the rock properties are assigned to the cells of the reservoir simulator with the same rock types.

Rock classification methods can be divided into two categories. The first category is based on empirical equations and uses the regression method to obtain parameters such as the Winland R35, Pittman (1992) and Aguilera (2002)

equations. The second category is a theoretical method using Kozeny's (1927)—Carman's (1937) equation with Darcy's law for flow in a porous medium and Poiseuille's law for flow in a tube as a basis to derive the formula. Kozeny (1927) and Carman (1937) simulated a porous medium as a bundle of capillary tubes. This ideal model dates back several decades. Amaefule *et al.* (1993) are pioneers in this work. They presented the flow zone indicator (*FZI*) method. Since 1940, several equations have been proposed, one of the most pioneering equations established by Leverett (1941), which aimed to predict water saturation (S_w) by correlating the three parameters S_w, P_c, and petrophysical parameters (Φ and k). Leverett also pioneered the normalization of capillary pressure curves by developing the famous J-function method for unconsolidated sandstone reservoirs. Later, Morris & Biggs (1967), Timur (1968), and Coates & Denoo (1981) proposed empirical equations (EEs) based on the correlation between permeability, porosity, and irreducible water saturation. These EEs apply only to irreducible water saturation and clean sandstone reservoirs. Overall, these formulas are used to calculate permeability from well log data and can only be used to obtain an order of magnitude for permeability (Balan *et al.* 1995). Dale Winland (1972), the AMOCO geologist studying the Spindle field sandstones in Colorado, introduced the Winland R35 method. Kolodzie (1980) and Pittman (1992) further developed Winland's work. Amaefule *et al.* (1993) confirmed that pore geometry variations result in separate zones with identical flow characteristics. They developed a method based on the Kozeny (1927), Carman (1937) equation using the concept of mean hydraulic radius. Routine core analysis (RCAL) is used to characterize the permeability and porosity of the rock sample and determine the reservoir quality index (RQI) and FZI. The FZI method has been used as a desirable method in various studies since Amaefule *et al.* (1993) introduced this method based on the permeability and effective porosity ratio (Guo *et al.* 2007; Shabaninejad 2011; Rahimpour-Bonab *et al.* 2012; Soleymanzadeh *et al.* 2019). Nooruddin & Hossain (2011) modified the FZI method by introducing FZI_m based on the Kozeny–Carman model and the cementation factor. Izadi & Ghalambor (2013) introduced FZI_{IG} by substituting $R\sqrt{1 - S_{wir}}$ in place of r in the Kozeny–Carman equation, where R is the nominal radius of the capillary tube. Mirzaei-Paiaman *et al.* (2015) introduced FZI* based on the Kozeny–Carman equation, Poiseuille's equation, and Darcy's law. The FZI* is obtained by replacing rmh with r in the Kozeny–Carman equation, where rmh is the effective or mean hydraulic unit radius. The data obtained from combining petrophysical, geological, and statistical analyses can be converted into hydraulic flow units (HFU) and correlated with well log results to produce regression models for permeability estimates in core-free zones. Gunter *et al.* (1997) confirmed the importance of studies on HFUs. These stud-

ies are needed to understand reservoir behavior. Shedid & Almehaideb (2002) considered that the structure and geometry of the pore size and pore throats have a directional influence on the capillary pressure curves. For a more accurate classification, Shedid & Almehaideb (2002) focused on the lithology of the rocks. They classified core samples based on their lithology and petrophysical properties. They developed a new technique to adequately describe the classification of carbonate rocks, called the characterization number (*Cn*). This method combines the significant variables of porous media, such as permeability, porosity, pore size, fluid properties, and interactions between the reservoir rock and the fluids flowing through it (i.e. contact angle).

One approach for rock-type classification is to combine porosity obtained from well logging with the FZI method and a synthetic log for predicting rock permeability (Siddiqui *et al.* 2003, 2006; Ye *et al.* 2011; Ghadami *et al.* 2015; Riazi 2018; Soleymanzadeh *et al.* 2018). Dakhelpour-Ghoveifel *et al.* (2019) described a method for rock typing in the transition zone of a carbonate reservoir. They explained the observed variation in water saturation data versus depth and how rock types can be assigned to transition zone grids. The objective of the capillary-based method is to produce a map of water saturation that incorporates both laboratory and well log data and includes depth so that it can adequately account for the transition zone. Recent developments in rock typing have focused on dynamic rock typing. An approach to dynamic rock typing is proposed by defining a true effective mobility tool (TEM-function) to convert relative permeability data to fluid flow indicators (Mirzaei-Paiaman *et al.* 2019b).

This paper focuses on reservoir rock classification in the Ahvaz Asmari and Mansouri oilfields based on water–oil PDCP by applying the modified empirical equation (MEE) technique and calculating permeability from well log data. The MEE is proposed based on porosity, permeability, and irreducible water saturation. Several EEs between S_{wi}, Φ, and k are introduced to calculate k for sandstone reservoirs (equations (8), (10), and (12)). However, a limitation of these equations is that the reservoirs have irreducible water saturation. In addition, the equations are not used for rock-type classification and can only be used to estimate permeability from well log data.

Since 1940, several studies have been conducted to explain rock-type classification, but it is still a significant open problem. There have been problems finding a method for rock-type classification that includes irreducible water saturation. This study provides a new insight into the process and gives a better conception of the procedure. In addition, this study improves the current understanding of rock-type classification by using irreducible water saturation and provides the solution for the problem that it suffers. This study fills the gap between the technique with and without irreducible water saturation.
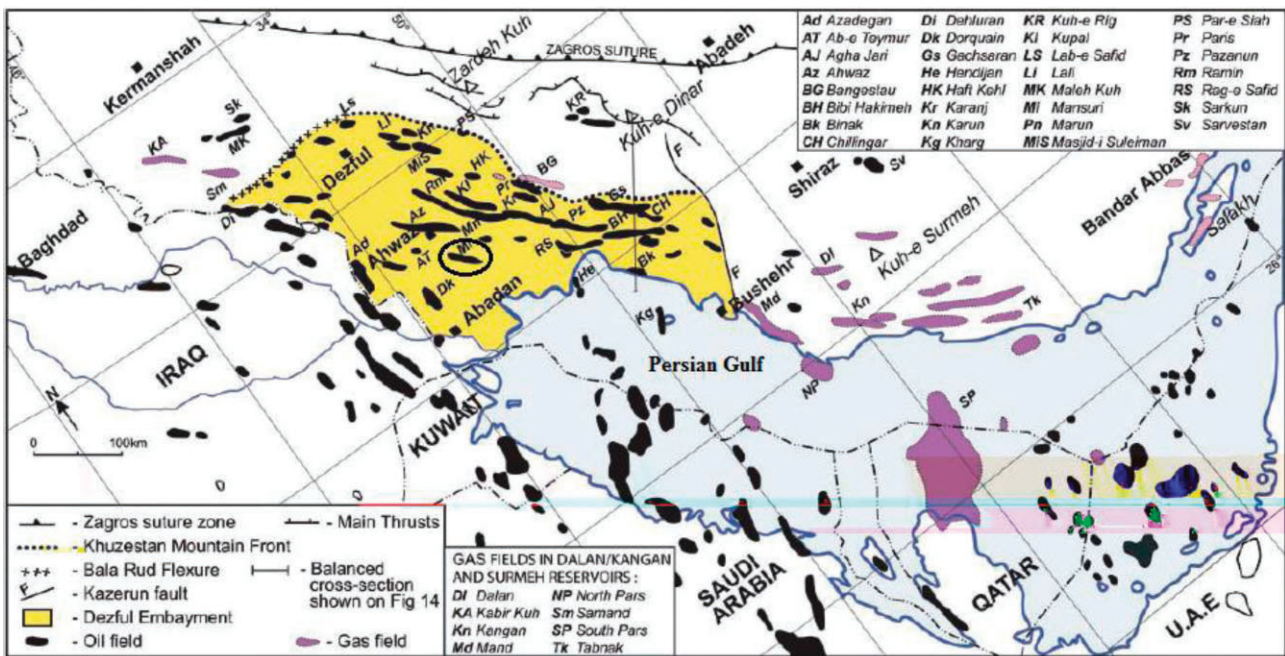
Figure 1. Ahvaz and Mansouri oilfield location map in the Dezful depression region (Bordenave & Hegre 2005).

2. Oilfield description

We use data from two oilfields from southwest Iran to examine the new method presented in this article. Here, we describe these two oilfields.

2.1. Ahvaz Asmari oilfield

The Ahvaz Asmari oilfield in southwest Iran is located in the Dezful depression region and has a northwest–southeast trend parallel to the Zagros mountain range. The average length of the Ahvaz oilfield is 80 km and its width is ∼10 km. The Ahvaz oilfield has an anticline structure and is considered one of the last parts of the folded Zagros region. This anticline is located on a ridge (Horst) that occurred in the older classes. The Ahvaz oilfield anticline is more or less symmetric. The quality of the Ahvaz Asmari reservoir is generally enhanced by a system of fractures that occur near the tops of high-relief anticlines. The basal part of the Ahvaz Asmari is sandy, which shows increased porosity in the southwest of the Dezful Embayment. The Ahvaz Asmari cap rock is the thick evaporates of the Gachsaran formation with an effective seal. The entrance to the anticline of the Ahvaz Asmari Formation is ∼2500 subsea level meters, with the Asmari Formation 250 to 500-m thick (Bordenave & Hegre 2005; Rabbani &Tirtashi 2010; Opera *et al.* 2013; Moradi *et al.* 2017).

The Ahvaz Asmari reservoir is divided into 10 layers. Layers A-1, A-3, A-5, and A-7 are carbonate rocks with shale and sand. Layers A-10 and A-11 are mainly shales with sand, and the other layers are mostly sand with shale. The carbonate

formation consists of anhydrite, dolomite, lime, dolomitic lime, and shale limestone dolomites. The sandstone formation consists of sandstone (quartz arenite and quartz wacke) and sandstone–shale with poor to loose cement, and good textural maturity generates highly porous and permeable zones (Haidari *et al.* 2020). The great variety in the rock types of the Ahvaz Asmari oilfield has resulted in a very heterogeneous reservoir with high complexity in its static characteristics and dynamic behavior. The Ahvaz Asmari oilfield was discovered in 1959 by drilling well number 6 and now has >250 producing wells with a production rate of 600 000 barrels/day. The recoverable hydrocarbon is estimated as 10 billion barrels of oil and 13 trillion cubic feet of gas (Rabbani &Tirtashi 2010). The water drive mechanism governs the Ahvaz Asmari oilfield. The flow of water from west to the east helps maintain the reservoir pressure. The average porosity of the Ahvaz Asmari oilfield is 18%, it has API degrees of ∼30, and is one of the largest oil-producing reservoirs in Iran (Speight 2014). Figure 1 shows the location map of the Ahvaz and Mansouri oilfields in the Dezful depression region.

2.2. Mansouri oilfield

The Mansouri oilfield in southwest Iran is located in the Dezful depressed region adjacent to the Ahvaz oilfields. The average length of the Mansouri oilfield is ∼39 km, and its width is ∼5 km. The Mansouri oilfield consists of the Asmari, Bangestan, and Khami reservoirs. The Mansouri Asmari Formation mainly consists of sandstone. The Bangestan reservoir

includes the Ilam and Sarvak formations and commonly consists of carbonate rocks as the upper and lower reservoirs, respectively (Soleimani *et al.* 2018). The Mansouri oilfield was identified using geophysical methods in 1962 and, the same year, drilling Well No. 1 was discovered, and production started after installing production facilities in 1974. The amount of Asmari oil in place is estimated at ∼3.3 billion barrels, and its oil production is ∼110 000 barrels per day. The Mansouri oilfield has a heterogeneous reservoir with high complexity in its static characteristics and dynamic behavior. Bangestan is estimated to hold 15 billion barrels of oil with an output of 60 000 to 79 000 barrels per day. Oil production from the Bangestan reservoir began in 1974 after drilling Well No. 2.

3. Materials

3.1. FZI method

The FZI method has been extensively used for rock-type classification. The mean hydraulic radius and the modified Kozeny–Carman equation are used as conceptual criteria for classifying rock types. Amaefule *et al.* (1993) presented a correlation as follows:

$$RQI = \Phi_z \times FZI, \qquad (1)$$

$$RQI = \sqrt{\frac{k}{\Phi_e}}, \qquad (2)$$

$$\Phi_z = \frac{\Phi_e}{1 - \Phi_e}, \qquad (3)$$

$$FZI = \frac{1}{\sqrt{F_s}\, \tau S_{gv}}, \qquad (4)$$

where k is in μm^2, Φ_e is in fraction, τ is the tortuosity coefficient, Φ_e is the effective porosity, S_{gv} is the surface area per unit grain volume, and F_s is the shape factor, which is equal to 2 for spherical particles. Equation (1) can be used as an index to classify rock types and can be written as follows:

$$FZI = \frac{RQI}{\Phi_z} = \frac{1}{\Phi_z}\sqrt{\frac{k}{\Phi_e}}, \qquad (5)$$

where FZI is expressed in µm.

The value of FZI should be the same for rocks in a category. Discrete rock types (DRTs) are applied to convert decimal numbers to integer numbers to provide a more accessible index for separating data (Shenawi *et al.* 2007). DRT is not a rock typing method and is only used to round

a real number to an integer. Nabawy & El Sharawy (2015) modified the DRT equation as follows.

$$DRT = Round\,(2 \times \ln\,(FZI) + 10.6; 0)\,. \qquad (6)$$

To study the separation and grouping of P_c curves, famous and valuable rock-type (RT) calcification indicators such as the Winland R35, Ghanbarian Index, Ngo Index, FZI, FZI*, FZI**, FZI$_{IG}$, and FZI$_m$ can be used. The discussion of these methods is available in the literature, therefore, they are not explained here. We compare the results of the *Cn* method with the FZI method, a well-known method in the literature.

3.2. Geostatistical analysis

In this study, we present statistical analysis to perform further investigation of the *Cn* method. Statistical analysis is the science of collecting data to discover unknown patterns and trends. The statistical analysis provides an approximation of an unknown parameter that is difficult or impossible to measure. In the context of geology, geostatistics helps to better characterize hydrocarbon reservoirs. A histogram or probability density function contains the necessary information about the details of the variables under study and shows a picture of the statistical population. It is done by introducing data as representatives of the statistical population. Three main categories of criteria are used to study the histogram or probability density function of samples:

(i) The center of the probability density function (i.e. mean, median).
(ii) The dispersion around the center of the probability density function (i.e. the variance or standard deviation).
(iii) The shape of the probability density functions compared to a standard probability density function (i.e. skewness coefficient, degree of asymmetry, and kurtosis coefficient).

Geostatistical analysis is used to support the MEE theory. For this purpose, the probability density functions of Φ, k, $|\ln(k)|$, $\sqrt{\frac{k}{\Phi}}$, and $\sqrt{\frac{|\ln(k)|}{\Phi}}$ are plotted in figure 2 according to the RCAL experimental data of ∼100 sandstone and carbonate core samples with different lithologies from eight wells of the Ahvaz Asmari and Mansouri oilfields. As shown in figure 2, these amounts of data are enough to obtain the trend (see Appendix A).

Since the data are collected from a variety of carbonate and sandstone lithologies, cover a wide range of lithologies, and have a sufficient population, the data are comprehensive and their generality can be inferred. As shown in figure 2a, the porosity histogram is close to the normal probability
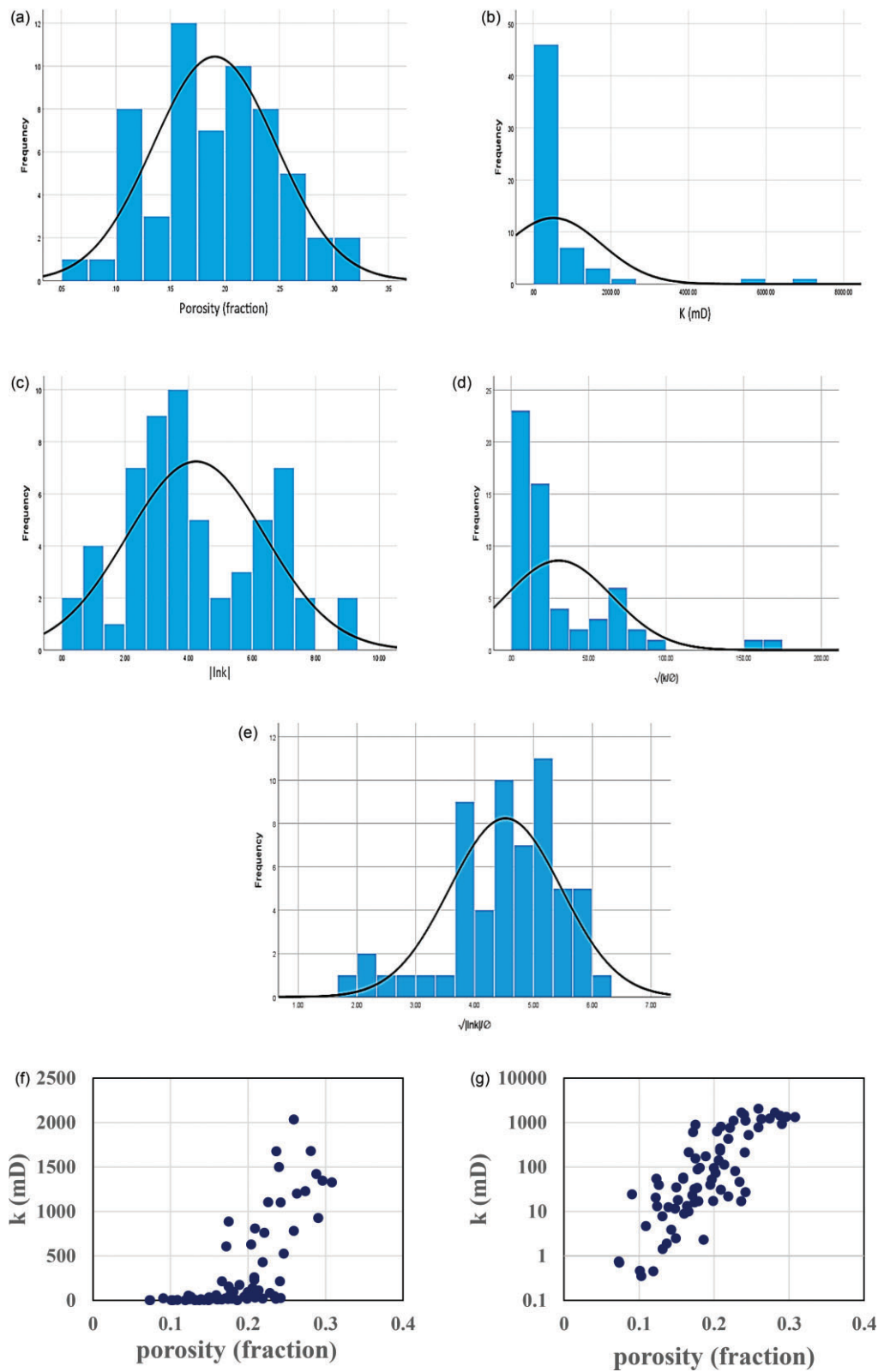
Figure 2. Histogram of (a) Φ, (b) k, (c) $|\ln(k)|$, (d) $\sqrt{\frac{k}{\Phi}}$, (e) $\sqrt{\frac{|\ln k|}{\Phi}}$, (f) plot of k vs Φ on Cartesian scale, and (g) plot of k vs Φ on semilogarithmic scale.

density pattern. However, the permeability histogram is right-skewed and deviates from the normal probability density pattern (figure 2b). The absolute logarithmic transformation is used for the permeability values to solve this problem (Amyx *et al.* 1960; Willhite 1986; Kelkar & Perez 2002). As shown in figure 2c, the $|ln(k)|$ distribution is more symmetric than the k distribution. As shown in figure 2a and c, the Φ histogram and the $|ln(k)|$ histogram are remarkably similar. This similarity indicates that there is a relationship between Φ and $|ln(k)|$. Figure 2d shows the histogram of $\sqrt{\frac{k}{\Phi}}$ used in the FZI method (see equation (5)), and figure 2e shows the histogram of $\sqrt{\frac{|ln(k)|}{\Phi}}$ used in the MEE (see equation (13)). As shown in figure 2d and e, the probability density pattern $\sqrt{\frac{|ln(k)|}{\Phi}}$ is more symmetric than $\sqrt{\frac{k}{\Phi}}$. This means that there is a correlation or relationship between porosity and the absolute logarithm of permeability, and there is no linear correlation or relationship between porosity and permeability (Amyx *et al.* 1960; Willhite 1986; Kelkar & Perez 2002). It is a reason why in recent decades, researchers have been interested in plotting permeability versus porosity in semilogarithmic scale instant of Cartesian scale (see figure 2f and g). Note that k, permeability, Φ, porosity, and $\sqrt{\frac{k}{\Phi}}$, pore radius, have physical meaning, however, $|ln(k)|$ and $\sqrt{\frac{|ln(k)|}{\Phi}}$ only have mathematical meaning and the absolute natural logarithm $|ln|$ is only used as an operator, to transform permeability data that do not have a normal distribution to data that do have a normal distribution (Amyx *et al.* 1960; Willhite 1986; Kelkar & Perez 2002). The main message of this section is that $\sqrt{\frac{|ln(k)|}{\Phi}}$ has a normal distribution and is used to derive equation (13) in Appendix A.

4. Method

4.1. Empirical equations (EEs)

Permeability estimation of well log data has been a significant subject for reservoir engineers and petroleum geologists when core data are not available. We explain three equations to estimate permeability from well log data as follows.

Morris & Biggs (1967) proposed the following empirical equation for sandstone porous medium.

$$k = \left(\frac{awr \times \Phi^3}{S_{wi}} \right)^2, \qquad (7)$$

where *awr* depends on the type of hydrocarbon fluid, k is the permeability in mD, and Φ and S_{wi} are the porosity and irreducible water saturation in fractions, respectively. The value of *awr* is 250 for oil and 79 for dry gas. The following

equation is obtained for oil reservoirs:

$$\frac{\sqrt{k}}{\Phi^3} \times S_{wi} = 250. \qquad (8)$$

Timur (1968) proposed another similar empirical equation for sandstone porous medium as follows:

$$k = \frac{0.136 \times \Phi^{4.4}}{S_{wi}^2}, \qquad (9)$$

where k is in mD, and Φ and S_{wi} are in percent. Timur's (1968) equation is not dependent on the type of hydrocarbon fluid in the porous medium. We have:

$$\sqrt{\frac{k}{\Phi^{4.4}}} \times S_{wi} = 0.37. \qquad (10)$$

Coates & Denoo (1981) proposed another similar empirical equation for sandstone porous medium as follows:

$$\sqrt{k} = 100 \times \Phi e^2 \left(\frac{1 - S_{wi}}{S_{wi}} \right), \qquad (11)$$

where k is in mD, and Φ and S_{wi} are in fractions. The Coates & Denoo (1981) equation is not dependent on the type of hydrocarbon fluid in the porous medium. We have

$$\frac{\sqrt{k}}{\Phi e^2} \times \left(\frac{S_{wi}}{1 - S_{wi}} \right) = 100. \qquad (12)$$

Equations (8), (10), and (12) all have the same basic form. These EEs include permeability, porosity, and irreducible water saturation. In addition, the right hand of these EEs is a constant value. To date, solid proof has not been presented for EEs; however, this has not caused a limitation in the use of these equations and these useful equations are still used to calculate the permeability from well log data. These useful EEs were used to obtain some ideas. The MEE is proposed based on the concepts obtained from these EEs.

4.2. Modified empirical equation (MEE)

The ratio of permeability to porosity has been used in the RT classification method. The porosity has a normal distribution pattern. The well-known rule in this area is that the permeability has a log-normal distribution, and thus, $|ln(k)|$ follows a normal distribution pattern (Amyx *et al.* 1960; Willhite 1986; Kelkar & Perez 2002) (see Section 3.2). The value of k differs from the value of $|ln(k)|$ based on mathematical concepts and properties of natural logarithm. Similar to equations (8), (10), and (12) (exclusive relationships between k, Φ, and S_{wi}), the MEE is proposed based on the normal distribution pattern of Φ and $|ln(k)|$ (see Section 3.2 and figure 2a and c). Since $|ln(k)|$ and Φ have a normally distributed pattern, there is a relationship between $|ln(k)|$ and Φ. Therefore,

Table 1. Core and Cn data for the Ahvaz Asmari oilfield

No.	Well no.	Lithology	Sample no.	ϕ (fraction)	k (mD)	Swi (fraction)	Cn	Description
1	53	carbonate	10	0.241	213	0.052	0.25	CRT-1
2	53	carbonate	9	0.208	261	0.06	0.31	CRT-1
3	19	carbonate	6	0.214	112	0.075	0.35	CRT-1
4	89	carbonate	6	0.219	21.7	0.101	0.38	CRT-1
5	19	carbonate	7	0.178	34.1	0.09	0.39	CRT-1
6	53	carbonate	11	0.242	27	0.12	0.44	CRT-2
7	89	carbonate	8	0.186	2.3	0.223	0.46	CRT-2
8	19	carbonate	4	0.2	94.3	0.11	0.50	CRT-2
9	53	carbonate	2	0.131	7.8	0.138	0.54	CRT-2
10	53	carbonate	3	0.109	4.7	0.152	0.57	CRT-2
11	89	carbonate	7	0.195	40	0.14	0.61	CRT-2
12	53	carbonate	4	0.159	58	0.131	0.66	CRT-2
13	89	carbonate	5	0.209	30.9	0.187	0.74	CRT-2
14	53	carbonate	1	0.159	54	0.161	0.81	CRT-2
15	53	carbonate	18	0.164	13.3	0.247	0.98	CRT-3
16	53	carbonate	6	0.139	12.5	0.241	1.03	CRT-3
17	53	carbonate	12	0.152	18	0.25	1.09	CRT-3
18	53	carbonate	19	0.164	13.3	0.274	1.09	CRT-3
19	53	carbonate	17	0.174	32	0.274	1.22	CRT-3
20	53	carbonate	13	0.152	18	0.344	1.5	CRT-4
21	53	carbonate	7	0.122	20.3	0.319	1.58	CRT-4
22	53	carbonate	14	0.123	54	0.425	2.42	CRT-5
23	53	carbonate	15	0.123	54	0.464	2.64	CRT-5
1	19	sandstone	9	0.246	5900	0.065	0.39	SRT-1
2	89	sandstone	4	0.226	1105	0.075	0.42	SRT-1
3	89	sandstone	1	0.204	628	0.08	0.45	SRT-1
4	19	sandstone	8	0.261	7040	0.08	0.47	SRT-1
5	89	sandstone	3	0.274	1227	0.1	0.50	SRT-1
6	53	sandstone	5	0.171	2.3	0.124	0.53	SRT-1
7	89	sandstone	2	0.259	2035	0.11	0.62	SRT-2
8	19	sandstone	3	0.219	428	0.12	0.63	SRT-2
9	84	sandstone	5	0.288	1421	0.161	0.81	SRT-3
10	84	sandstone	6	0.281	1678	0.168	0.86	SRT-3
11	84	sandstone	4	0.308	1327	0.181	0.87	SRT-3
12	84	sandstone	1	0.175	887	0.18	1.12	SRT-3

$\sqrt{\frac{|ln(k)|}{\Phi}}$ also has a normally distributed pattern (see Section 3.2 and figure 2e), which means that divided $|ln(k)|$ to Φ follows the regular pattern. To obtain equation (13), $\sqrt{\frac{|ln(k)|}{\Phi}}$ is multiplied by S_{wi}. Equation (13) is used for RT classification and permeability estimation from well log data.

$$Cn = \sqrt{\frac{|ln(k)|}{\Phi}} \times S_{wi}, \qquad (13)$$

where k is permeability in mD, and Φ is porosity in fractions and S_{wi} is irreducible water saturation in fractions. *Cn* has a constant value for each rock type. Since reservoir permeability ranges from a few nano-Darcy to a hundred Darcy, $ln(k)$ is negative for formations with low permeability. Since the logarithm of permeability is negative for permeability values less than one, the absolute value is used in the numerator.

The main difference between the new method and previous EEs is the use of $|ln(k)|$ instead of k to obtain similar distribution functions for permeability (see Section 3.2). In addition, unlike the other EEs, *Cn* is a nonfixed value and has different values for different rock types. Proof for equation (13) based on a physical observation method is presented in Appendix A. Note that this is not solid basis proof. The method presented in this article categorizes on the basis of the methods that use EEs, such as the Winland R35, Pittman (1992) and Aguilera (2002) equations.

5. Method validation

5.1. Ahvaz Asmari oilfield

In this study, data on Φ, k, S_{wi}, and PDCP are used to classify the RT in carbonate and sandstone reservoirs. In addition,
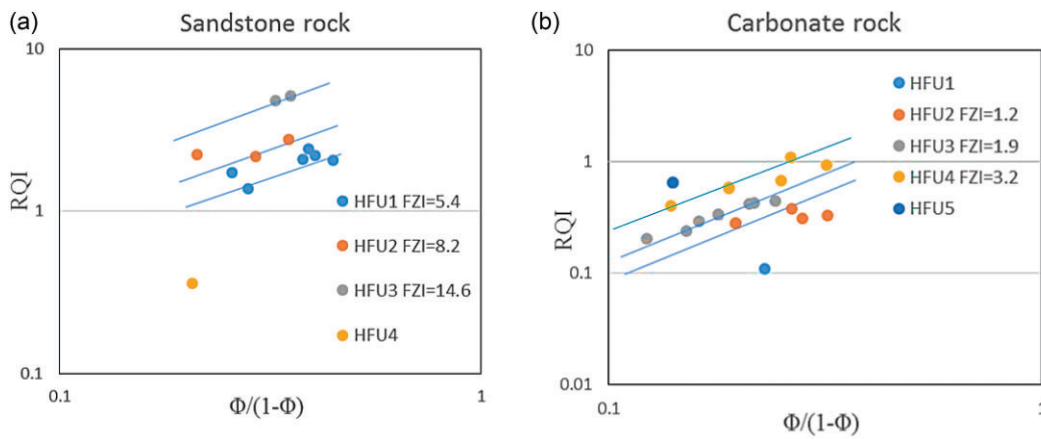
Figure 3. Plot of RQI against $\frac{\Phi}{(1-\Phi)}$ based on the DRT classification using the FZI method: (a) sandstone rock and (b) carbonate rock.
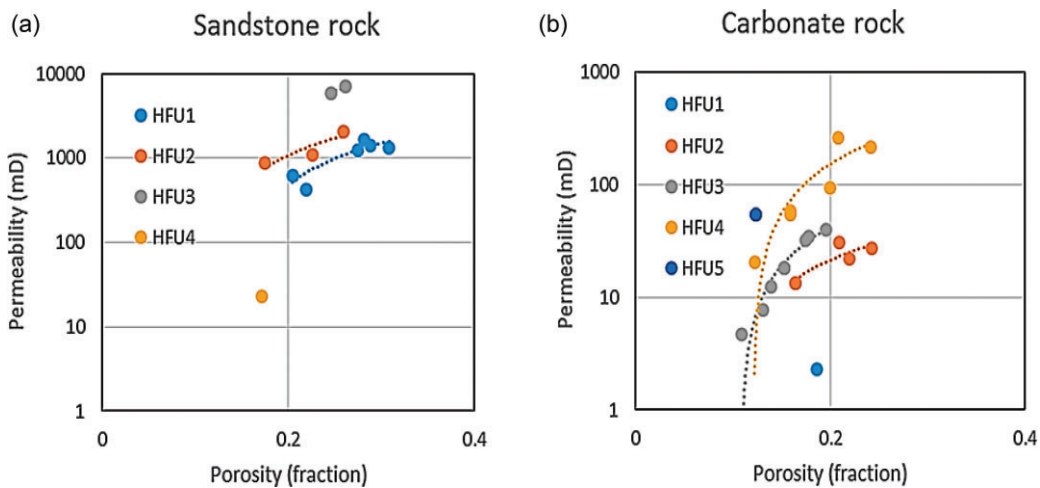

Figure 4. Plot of k against Φ based on DRT classification using the FZI method: (a) sandstone rock and (b) carbonate rock.

force imbibition capillary pressure and relative permeability are applied to complete the description of the RT classification. PDCP and force imbibition experimental data were obtained using a porous plate and centrifugal experiment, and the relative permeability was determined by an unsteady state experiment. Formation brine and oil were used for core experiments. The PDCPs were converted to reservoir conditions, assuming an interfacial tension between oil and brine in the reservoir of 30 dynes/cm. Porosity and permeability were obtained from RCAL tests. Values of reservoir rock properties (i.e. porosity, permeability, and irreducible water saturation) are shown in Table 1. Table 1 is sorted based on the increasing value of *Cn* for carbonate and sandstone lithologies.

Rock data are analyzed separately in two groups of sandstone and carbonate rock types. The routine experimental data from Table 1 (Φ and k) for sandstone and carbonate samples are classified using the FZI method. Accordingly, the samples are divided into four HFUs for sandstone and

five HFUs for carbonate lithologies resulting from equation (6). Substituting equation (3) into equation (1) and taking the logarithm, equation (14), is obtained as follows:

$$Log(RQI) = Log\left(\frac{\Phi}{1-\Phi}\right) + Log(FZI). \qquad (14)$$

When the RQI data are plotted against $\left(\frac{\Phi}{1-\Phi}\right)$, a straight line with a uniform slope appears on the log–log plot. The points on each line have the same FZI value, indicating that the flow units are the same and that the samples relevant to those points form a flow unit. The samples with the same HFU values fall into a cluster. Figure 3 shows the variation in RQI vs $\left(\frac{\Phi}{1-\Phi}\right)$ on a logarithmic scale for sandstone and carbonate samples. As shown, different groups can be identified by lines that have a slope of one. Note that in Figs 3a and 4a (sandstone rock), HFU4 (point 6 in Table 1, sandstone lithology) is far away from the prediction because of the low quality of rock property ($\Phi = 0.171$ and $k = 2.3$ mD) of this point
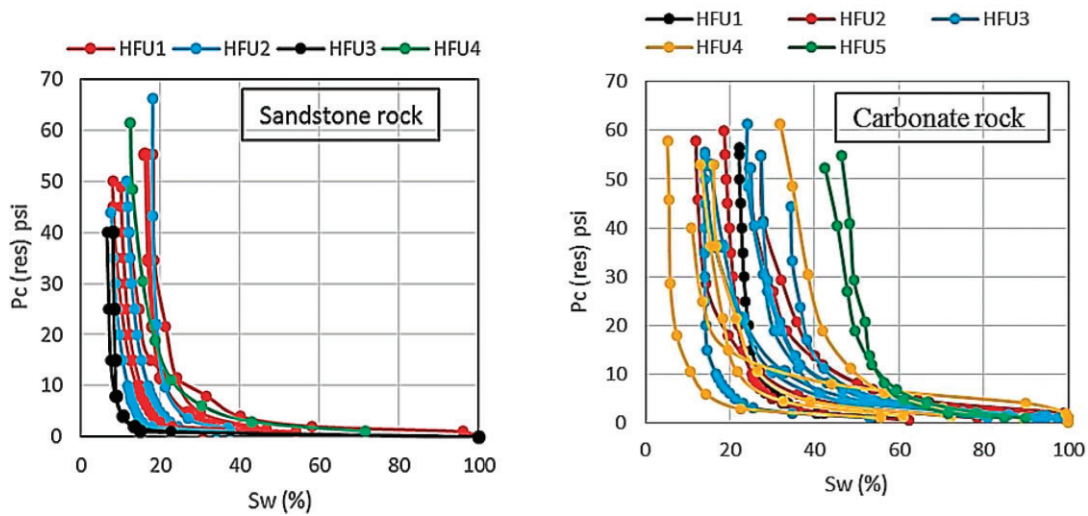
Figure 5. PDCPCs based on DRT classification using the FZI method: (a) sandstone rock and (b) carbonate rock.
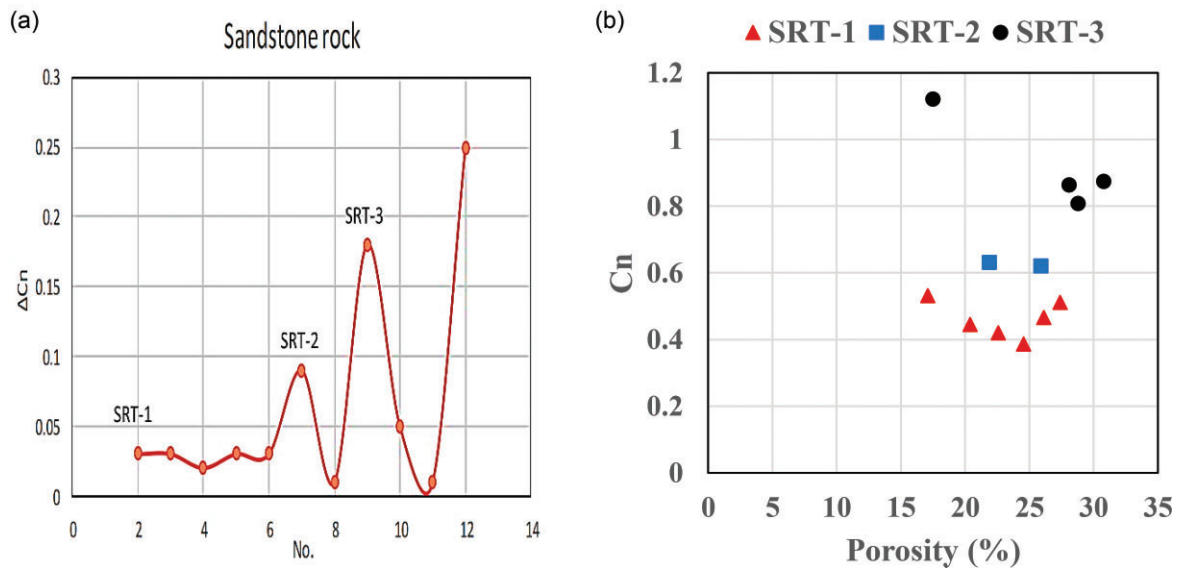

Figure 6. Classification of sandstone samples using the Cn method: (a) plot of ΔCn vs no. and (b) plot of Cn vs ϕ.

related to other sandstone points. In Figs 3b and 4b (carbonate rock), HFU1 (point 7 in Table 1, carbonate lithology) is far away from the prediction because of the low quality of rock property ($\Phi = 0.186$ and $k = 2.3$ mD) of this point related to other carbonate points. Results in figures 3 and 4 are stated intuitively to make sense of how rock types are selected.

Figure 4 shows the changes in permeability versus porosity for HFUs (sandstone rock samples figure 4a and carbonate rock samples figure 4b) on a semilogarithmic scale. Figure 4 is used to determine permeability from porosity for each HFU when the experimental data is not existed. The accuracy of permeability determines in figure 4 depends on the experimental data scattering for each HFU. If the

scattering for each HFU is low, the permeability determined in figure 4 is more accurate i.e. HFU3 in figure 4b.

The FZI method classifies rocks using routine data, i.e. Φ and k. Figure 5 shows the PDCPCs vs S_w for HFUs using the FZI method. Figure 5a shows the PDCPCs vs Sw for four sandstone HFUs. Figure 5b shows the PDCPCs vs Sw for five carbonate HFUs. Figure 5 shows intuitively how HFUs, P_c vs S_w are arranged relative to each other. According to figure 5, the curves overlap, which means the rock types cannot be selected using the FZI method.

In the *Cn* method, we assume the values *Cn* for each rock type are constant but are not fixed (see Table 1). It is a problem that the *Cn* method suffers it. Therefore, the rock samples with approximately the same values of *Cn* are
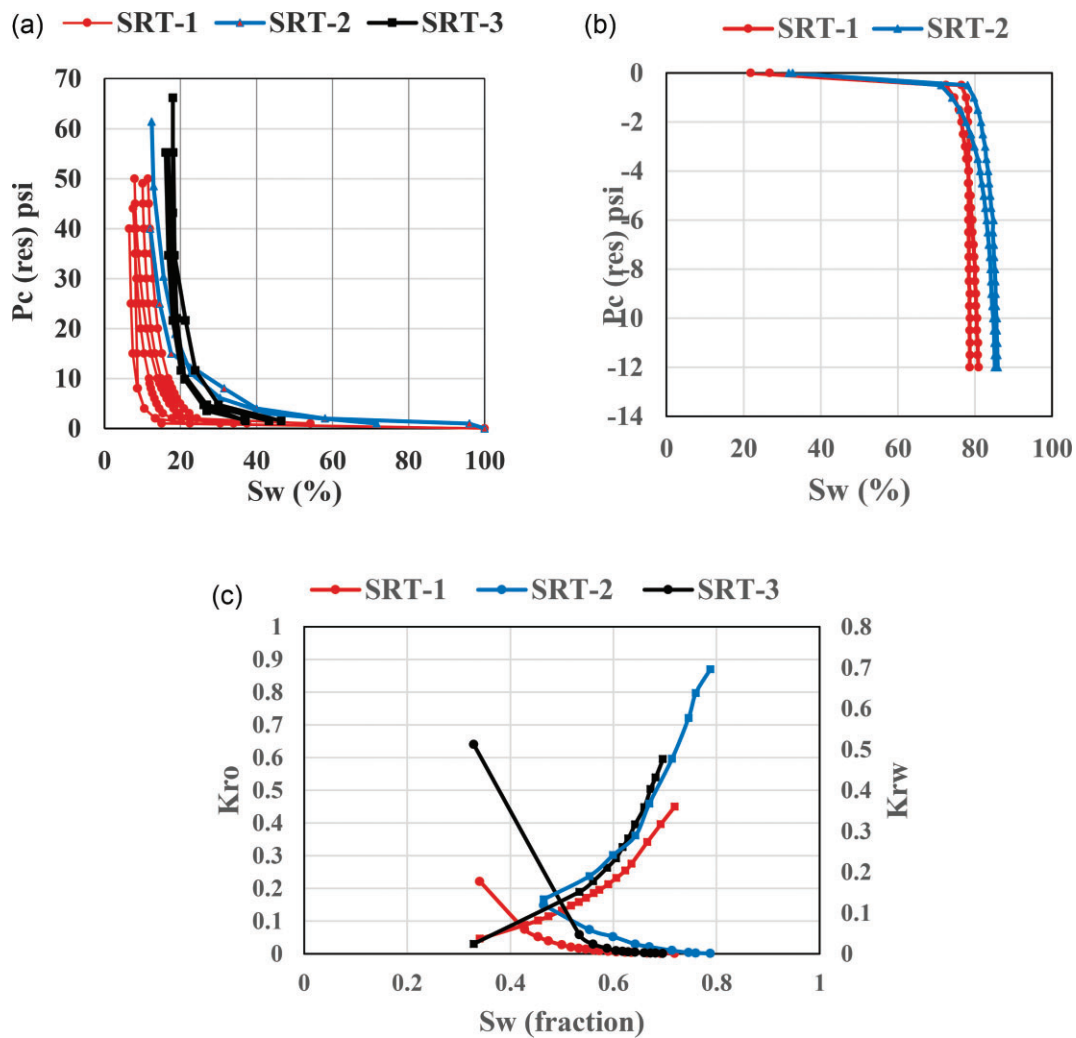
Figure 7. (a) PDCPCs of sandstone samples using the *Cn* method, (b) force imbibition capillary pressure, and (c) relative permeability. The circle symbol stands for the relative permeability of oil, and the square symbol stands for the relative permeability of water.

considered one rock type. The rock classification for the *Cn* method is based on Δ*Cn*. Figure 6a shows the plot of Δ*Cn* vs no. using data in Table 1. For example, ΔC_2 is calculated as 0.42–0.39 = 0.03, and No. is selected equal to 2. This data (2, 0.03) is chosen as one point for sandstone lithology (see figure 6a). For sandstone lithology, all data in Table 1 are calculated and plotted vs No. (see figure 6a). The maximum peak of Δ*Cn* is used to select the rock types (see figure 6a). In addition, *Cn* vs ϕ has also been plotted in figure 6b for more clarity of the rock types classification technique. Figure 6 uses the technique for selecting the rock types. Figure 7 shows the rock types classification results in the sandstone rock. Figure 7a shows the PDCPCs vs S_w for three sandstone rock types (SRTs) using the *Cn* method. It is self-evident for the two close rock types, i.e. SRT-1 and SRT-2, especially for points that are close to each other that close PDCPCs are overlapping, but for two farther rock types, i.e. SRT-1 and SRT-3, none of the PDCPCs must overlap (see figure 7a).

In addition, figure 7a shows intuitively how SRTs, Pc vs Sw arranged relative to each other. Figure 7b shows force imbibition capillary pressure corresponding to the PDCP. Figure 7c shows the relative permeability corresponding to the PDCP. These data are used in reservoir simulation.

As shown in figure 6, three different rock types can be identified using Δ*Cn* peak, i.e. SRT-1 from No. 1 to No. 6 and SRT-2 from No. 7 to No. 8 and SRT-3 from No. 9 to No. 12. The range of *Cn* values and the arithmetic average (arithmetic average is calculated from minimum to maximum value of *Cn* for each rock type, i.e. for SRT-1, arithmetic average is equal to (0.39 + 0.53)/2 = 0.46, see Table 1) for each sandstone rock type is shown in Table 2.

The same analysis was used for the carbonate rock. figure 8 shows intuitive carbonate rock type (CRT) selection. As shown in figure 8a, five CRTs can be selected using the *Cn* method. Figure 9 shows the results in the carbonate rock. Figure 9a shows the PDCPCs vs S_w for five CRTs using the *Cn*
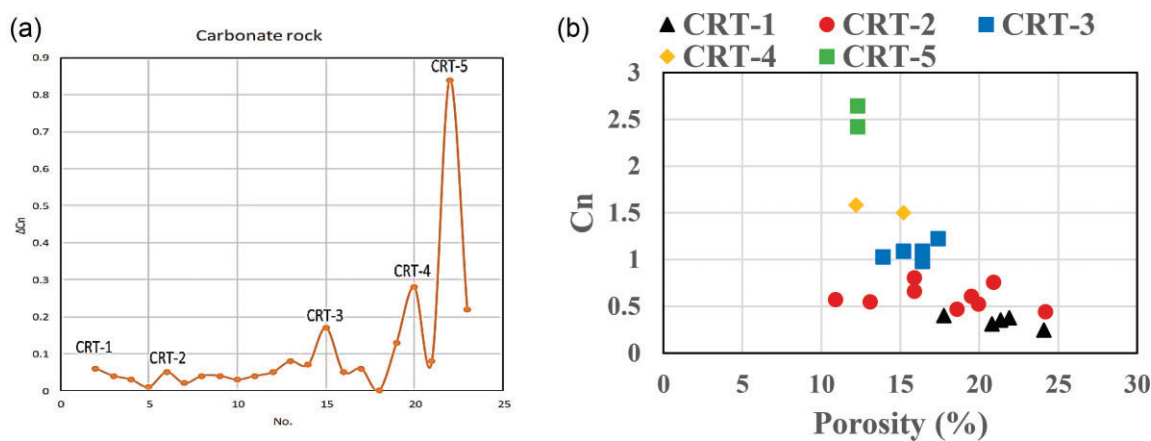
Figure 8. Classification of carbonate samples using the *Cn* method: (a) plot of Δ*Cn* vs no. and (b) plot of Cn vs φ.

Table 2. Sandstone rock types for the Ahvaz Asmari oilfield

Sandstone rock types	Range of Cn	Average of Cn
SRT-1	$0.3 < C1 < 0.6$	0.46
SRT-2	$0.6 < C2 < 0.8$	0.63
SRT-3	$C3 > 0.8$	0.92

method. In addition, figure 9a shows intuitively how CRTs, Pc vs Sw arranged relative to each other. Figure 9b shows force imbibition capillary pressure corresponding to the PDCP. Figure 9c shows the relative permeability corresponding to the PDCP. These data are used in reservoir simulation.

The range of *Cn* values and the average for each carbonate rock type are shown in Table 3.

Figures 7 and 9 show the PDCPCs for the sandstone and carbonate rock samples, respectively. According to Figs 7a and 9a, the curves do not overlap, which means that the rock types are correctly chosen. The data for water–oil force imbibition capillary pressure and relative permeability are limited, and they do not cover all sandstone and carbonate rock types. The available sandstone and carbonate data for rock are shown in figure 7b and c and figure 9b and c, respectively. The obtained results show that *Cn* method can accurately classify the rock types for both sandstone and carbonate reservoirs.

In the FZI method, the RT is selected based on all available data of *k* and Φ. In our technique, the RT is selected based on RCAL and special core analysis data, and PDCP data must be available. Therefore, in Figs 3 and 4, *k* and Φ, which have PDCP data, were used. In addition, the FZI method, as shown in Figs 3 and 4, is separately applied for sandstone and carbonate rocks to compare the results of the *Cn* method individually for sandstone and carbonate rocks (see figure 5a and b), shown in Figs 7a and 9a, with the FZI method. That is why the data used in Figs 3 and 4 are limited, although the results are explicit.

5.2. Mansouri oilfield

We applied the *Cn* method to classify the reservoir rock of the Mansouri oilfield to examine the performance and efficiency of the *Cn* method in another oilfield. As shown in Figs 10 and 11, the *Cn* method has good results in RT classification. The data of the Mansouri oilfield are shown in Table 4. Table 4 is sorted based on the increasing value of *Cn* for carbonate and sandstone lithologies.

6. Other applications

6.1. Determination of permeability from well log data

In this approach, permeability can be calculated from the well log data for each rock type. Rock types in core-free intervals can be classified and determined with nearby well core data. For the same rock type, using the known porosity and irreducible water saturation from the well log data in core-free intervals and *Cn*, the permeability can be calculated using equation (13). As a case study, we consider two nearby wells, i.e. wells A and B. Tables 5 and 6 show a section of lithology data of wells A and B, respectively.

Complete core data are available for well A, but in the interval from 2501.1 to 2527.9, the measured depth (MD) in well B is core free. The average permeability of well B in the interval from 2501.1 to 2527.9 MD can be calculated using average core data from well A in the interval 2581 to 2609.6 MD (i.e. $S_{wi} = 0.24$, $\Phi = 0.18$, and $k = 2.2$ mD). From equation (13), the value of Cn is calculated to be 0.5. Assuming that these two intervals (2501.1 to 2527.9 MD in well B and 2581 to 2609.6 MD in well A) have the same rock type, Cn has the same value for these two intervals. Using average well log data of well B for the interval 2501.1 to 2527.9 MD (i.e. $S_{wi} = 0.22$, $\Phi = 0.2$) and Cn = 0.5 (assuming the same rock type), the permeability from equation (13) is calculated to be 2.8 mD. The summarized data are presented in Table 7.
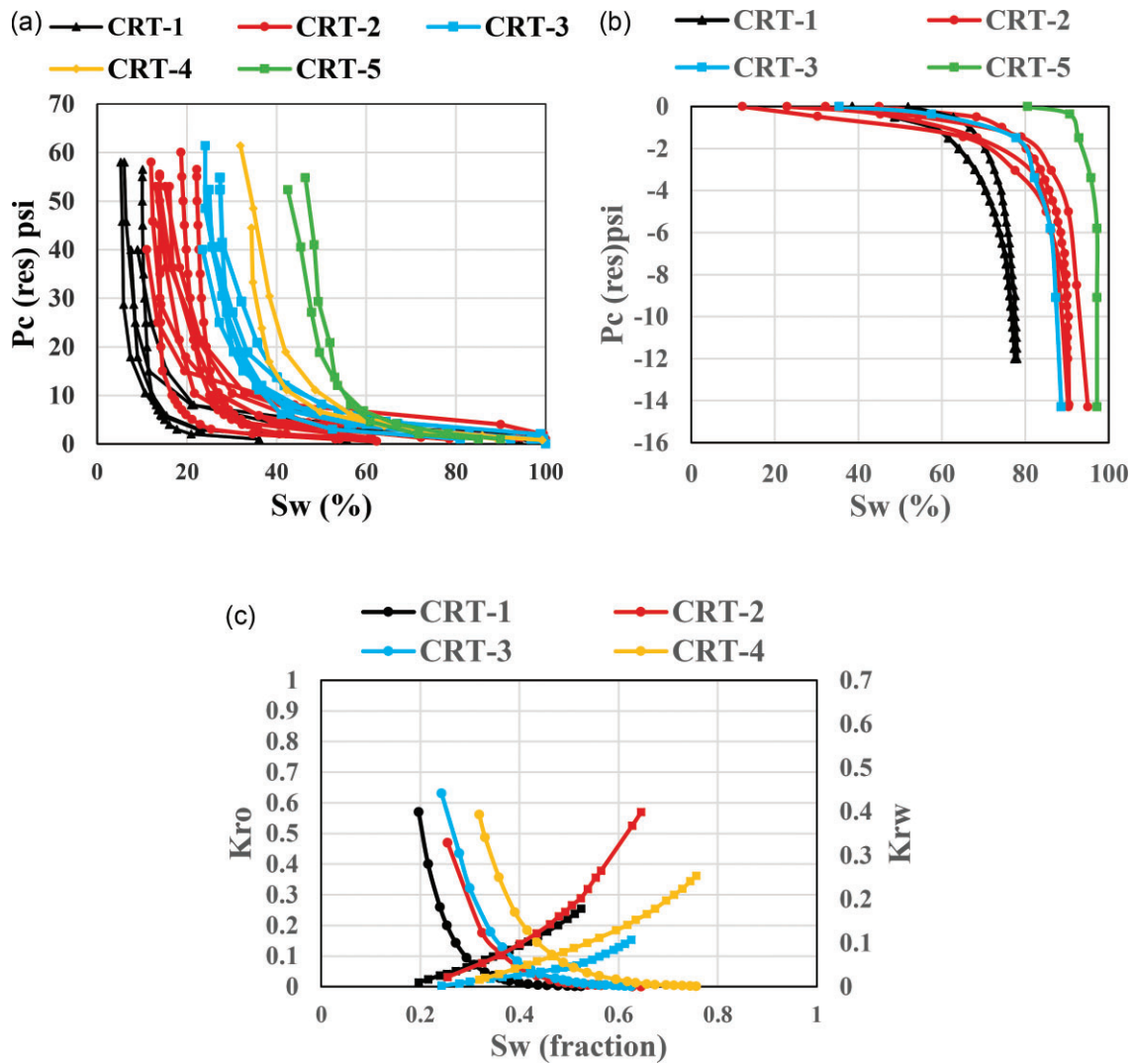
Figure 9. (a) PDCPCs of carbonate samples using the *Cn* method, (b) force imbibition capillary pressure, and (c) relative permeability. The circle symbol stands for the relative permeability of oil, and the square symbol stands for the relative permeability of water.

Table 3. Carbonate rock types for the Ahvaz Asmari oilfield

Carbonate rock type	Range of *Cn*	Average of *Cn*
CRT-1	0.24 < C1 < 0.4	0.34
CRT-2	0.4 < C2 < 0.8	0.6
CRT-3	0.8 < C3 < 1.2	1.08
CRT-4	1.2 < C4 < 1.6	1.54
CRT-5	C5 > 1.6	2.53

6.2. Determine the rock type when the formation water saturation is greater than the irreducible water saturation

In the oil zone, water saturation from well log data is assumed to correspond to irreducible water saturation. Thus, the rock type can be identified without difficulty. At this point, a critical question arises for classifying rock types based on irreducible water saturation: how do we select a rock type whose formation water saturation is more than the irreducible water saturation? The answer is as follows:

This begins with Archie's equation:

$$S_w^n \times \Phi^m = \frac{aR_w}{R_t}, \tag{15}$$

where *m* is the cementation factor, *n* is the saturation exponent, *a* is the tortuosity factor, and R_w and R_t are the formation water resistivity at the formation temperature and true resistivity of the formation in $\Omega \, m^{-1}$, respectively. In recent years, much research has been done to calculate the correlation between permeability and porosity. Among them, we can mention the project that was carried out by Saner *et al.* (1997) using 75 cores in one of the Saudi Arabia reservoirs. This relationship is one of the few relationships that can be used for sandstone and carbonate reservoirs. We suggest
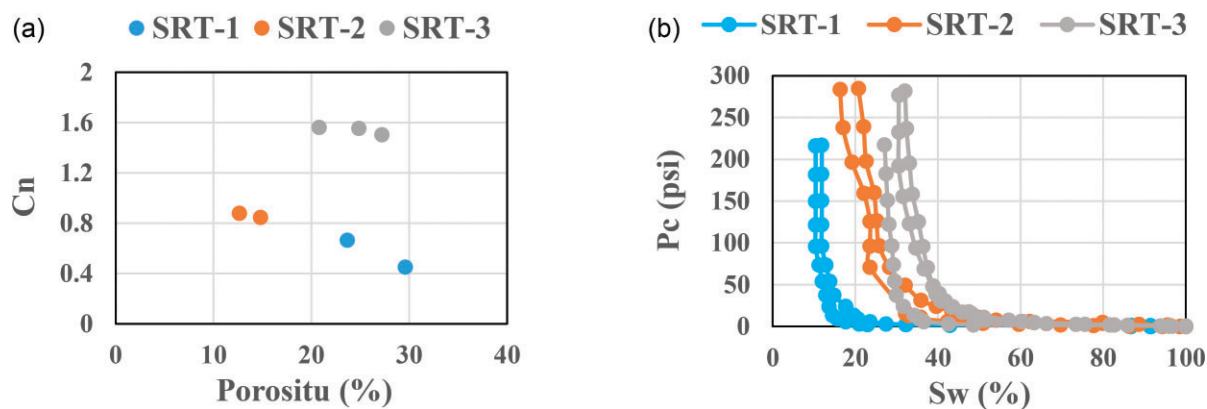
Figure 10. (a) Classification of sandstone samples using the *Cn* method. (b) PDCPCs of sandstone samples using the *Cn* method.
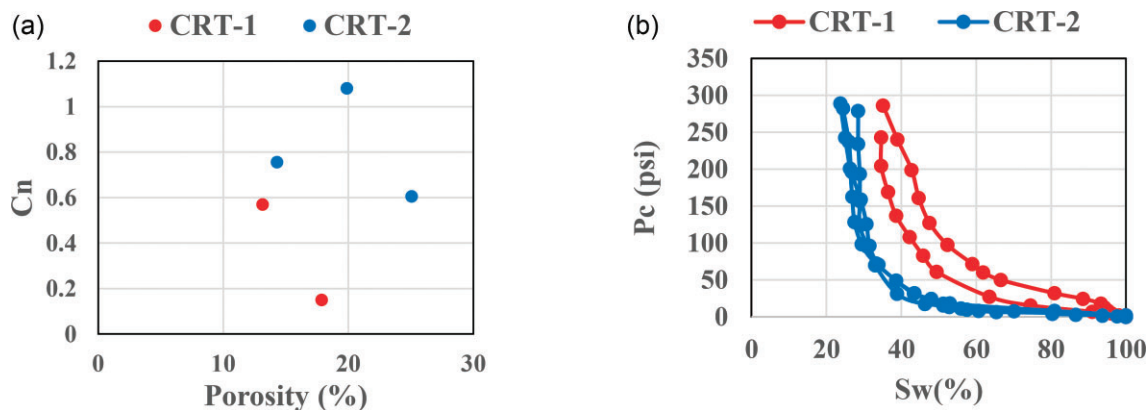

Figure 11. (a) Classification of carbonate samples using the *Cn* method, and (b) PDCPCs of carbonate samples using the *Cn* method.

Table 4. Core and *Cn* data for the Mansouri oilfield

No.	Well no.	Lithology	Sample no.	ϕ (fraction)	k (mD)	S_{wi} (fraction)	Cn	Description
1	60	carbonate	1	0.179	1.03	0.35	0.15	CRT-1
2	60	carbonate	6	0.131	1.43	0.347	0.57	CRT-1
3	60	carbonate	2	0.251	5.1	0.238	0.61	CRT-2
4	60	carbonate	8	0.143	3.9	0.245	0.75	CRT-2
5	60	carbonate	4	0.199	17.2	0.285	1.08	CRT-2
1	60	sandstone	5	0.30	1345	0.09	0.45	SRT-1
2	60	sandstone	10	0.24	1675	0.12	0.66	SRT-1
3	60	sandstone	8	0.15	11.5	0.21	0.84	SRT-2
4	60	sandstone	7	0.126	39	0.163	0.88	SRT-2
5	60	sandstone	3	0.272	403	0.32	1.5	SRT-3
6	60	sandstone	6	0.249	3636	0.27	1.55	SRT-3
7	60	sandstone	4	0.208	230	0.30	1.56	SRT-3

using the correlation between permeability and porosity from the data of the oilfield that is under study, which helps to obtain better results. The Saner *et al.* (1997) equation is as follows:

$$k = 0.008 \times 10^{0.166 \times \Phi}, \quad (16)$$

Assuming $m = n = 2$ in equation (15) (*a*, *m*, and *n* should be calculated for each RT). Substituting equation (15) and equation (16) into equation (13), we obtain:

$$C_n^2 = \frac{|ln(0.008 \times 10^{0.166 \times \Phi})|}{\sqrt{\frac{aR_w}{R_t}}} \times S_{wi}^2. \quad (17)$$

Table 5. Section of lithology data of well A (lithology in a volumetric percentage)

Depth (m)	Anhydrite	Limestone	Dolomite	Shale	Sandstone
2567.5	89	-	-	11	-
2568.5	91	-	-	9	-
2569.5	96	-	-	4	-
2570.5	100	-	-	-	-
2571.5	100	-	-	-	-
2572.5	54	-	36	-	-
2573.5	100	-	-	-	-
2574.5	100	-	-	-	-
2575.5	100	-	-	-	-
2576.5	100	-	-	-	-
2577.5	-	-	94	6	-

Table 6. Section of lithology data of well B (lithology in a volumetric percentage)

Depth (m)	Anhydrite	Limestone	Dolomite	Shale	Sandstone
2487.7	-	-	-	15	85
2488.7	-	-	-	15	85
2489.7	97	-	-	3	-
2490.7	100	-	-	-	-
2491.7	1.00	-	-	-	-
2492.7	100	-	-	-	-
2493.7	100	-	-	-	-
2494.7	100	-	-	-	-
2495.7	1.00	-	-	-	-
2496.7	100	-	-	-	-
2497.7	65	-	25	10	-

Table 7. Summarized data used to calculate the permeability from well log data

	Well A	Well B
Type of data	Core data	Well log data
Interval (MD)	2581 to 2609.6	2501.1 to 2527.9
k (mD)	2.2	2.8 (from equation (13))
Φ (fraction)	0.18	0.2
S_{wi} (fraction)	0.24	0.22
Cn (from equation (13))	0.5	0.5 (same rock type)

Equation (17) shows the relationship between S_{wi} and S_w. Equation (17) can be used to determine the value of S_{wi} for each sample when the formation water saturation is greater than the irreducible water saturation. A sample with an unknown rock type is first assumed to belong to rock type 1. The values of C1 and S_{wi} are determined from the RT classification, and $\frac{\sqrt{\frac{aR_w}{R_t}}}{S_w}$ and Φ are determined from well log data. From equation (17), Cn is calculated. If the calculated value

is equal to C1, the correct rock type is selected. Otherwise, the same calculations should be performed for the next rock type (i.e. the second rock type, C2). The flowchart of the process is shown in figure 12.

More detailed explanations are given as follows. As shown in figure 13, the sandstone formation is divided into two sections at the interval of 3904 to 3944 m. A section of lithology data from the well is shown in Table 8.

Figure 13 shows a part of the reservoir used to explain the case study. The green color (3904 to 3914 m) represents the oil zone, and the white color (3919 to 3934 m) represents the water zone. Let us first assume that these sections have the properties of SRT-1 (Table 1, k = 1105 mD, Φ = 0.226, S_{wi} = 0.075, Cn = 0.42). For the section containing water, S_w is determined from well log data equal to 0.6. To calculate Cn using the value of S_w instead of S_{wi} in Equation (13) results in 3.34. This value of Cn results in incorrect classification of rock type. To obtain the correct value of Cn, Equation (17) can be used. Using R_w = 0.05 ($\Omega\,\mathrm{m}^{-1}$), R_t = 20 ($\Omega\,\mathrm{m}^{-1}$), Φ = 0.20, and Sw = 0.6 from the well log data, S_{wi} = 0.075 from SRT-1, and a = 1, Cn is calculated to be 0.57 using Equation (17). These values of Cn (i.e. 0.42 and 0.57) can be assigned to the same rock type. Using Cn = 3.34 (calculated from Equation (13) using S_w instead of S_{wi}) shows a significant difference and incorrectly assigns this sample to a different rock type. The summarized data are presented in Table 9.

7. Limitations and suggestions

The generated results in this study are limited to the Ahvaz Asmari and Mansouri sandstone and carbonate formations. The FZI method, a famous RT classification method, was applied to compare the quality of the results. We expect Cn method to work efficiently in other reservoirs because of its robust performance. Therefore, we suggest that the Cn method applies to other reservoirs and compare with other RT classification methods, some of which cited in this paper.

8. Conclusion

This study presents the Cn method to classify rock types and calculate permeability from well log data for carbonate and sandstone rocks. The following conclusions are drawn from the results of this study:

(i) A Cn method has been introduced for rock typing based on permeability, porosity, and irreducible water saturation.

(ii) The Cn method was successfully used to classify the rock type of two heterogeneous carbonate and sandstone reservoirs in southwest Iran. The results show the rock type classification of the Cn method is a
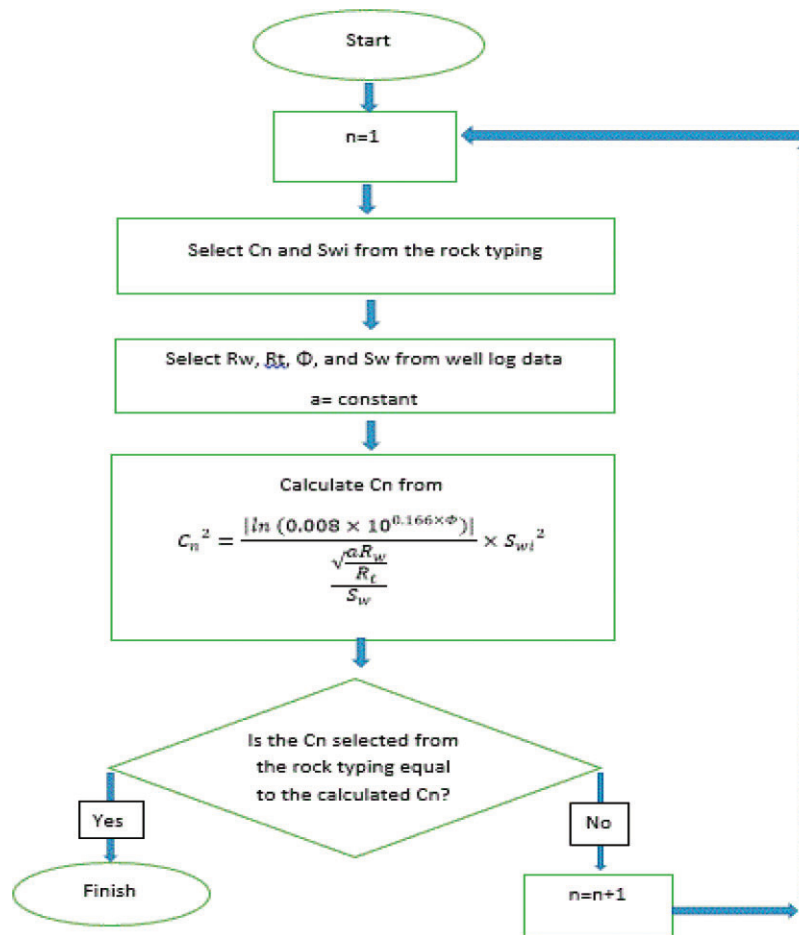
Figure 12. Flowchart for determining rock type when S_w is greater than S_{wi}.
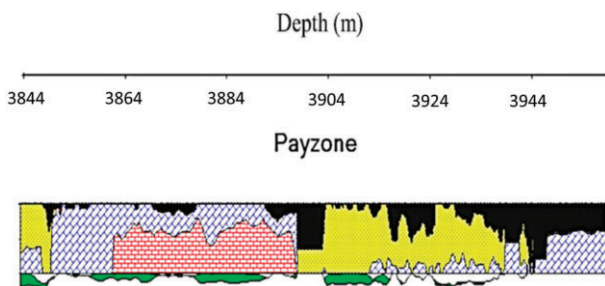

Figure 13. Section of the well log diagram, yellow is sandstone, red is dolomite, blue is limestone, and black is shale.

Table 8. Section of lithology data of well (lithology in a volumetric percentage)

Depth (m)	Anhydrite	Limestone	Dolomite	Shale	Sandstone
3903.9	-	-	-	66	34
3408.8	-	-	-	66	34
3905.7	-	-	-	66	34
3906.7	-	-	-	66	34
3907.6	-	-	-	-	100
3908.5	-	-	-	-	100
3909.4	-	-	-	-	100
3910.3	-	-	-	6	94
3914.9	-	12	-	-	88
3915.8	-	18	-	34	48
3916.7	-	10	-	54	36

significant advance compared to the *FZI* method and confirm the *Cn* method is a robust method to rock type classification.

(iii) The *Cn* method was used to calculate the permeability from well log data using porosity, irreducible water saturation, and *Cn*. The result shows the *Cn* method allows accurate calculation of permeability from well log data.

(iv) The *Cn* method is a simple and efficient approach to rock type classification.

(v) The *Cn* method was used to classify rock types when the formation water saturation exceeds the irreducible water saturation.

Table 9. Summarized data for determining rock type when formation water saturation is more than irreducible water saturation

Rock data selection	SRT-1 (Table 1) (oil zone)	Well log data (water zone)
Interval (m)	3904 to 3914	3919 to 3934
k (mD)	1105	1105
Φ (fraction)	0.226	0.20
S_{wi} (fraction)	0.075	-
S_w (fraction)	-	0.6
Cn (from equation (13))	0.42	3.34
Cn (from equation (17))	-	0.57
m	-	2
n	-	2
a	-	1
R_w ($\Omega\,m^{-1}$)	-	0.05
R_t ($\Omega\,m^{-1}$)	-	20

(vi) The role of irreducible water saturation in rock typing has been investigated.

Appendix A: Deriving equation (13) based on an experimental observation method

The experimental observation method has been used to find a relationship between parameters for physical phenomena. For example, Darcy's equation (1856), one of the essential equations in petroleum engineering, uses experimental observations of flow to obtain permeability.

Equation (13) is derived based on an experimental observation method and geostatistical analysis (see Section 3.2). We chose two main equations in the general form, which are found from the data shown in figure A.1a and b. From figure A.1a and b, two essential, acceptable and irrefutable physical concepts can be deduced from the conventional reservoir. As shown in figure A.1a, the permeability increases with increasing porosity, and as shown in figure A.1b, the irreducible water saturation decreases with increasing porosity. These two experimental observation concepts are used to derive Equation (13).

The equations chosen from figure A.1a and b are as follows:

$$|\ln(k)| = a\Phi^{c_1},$$

(Permeability increases with increasing porosity) (A.1)

a and c_1 are constants; $S_{wi} = b\Phi^{-c_2}$

(irreducible water saturation decreases with *increasing porosity*) (A.2)

b and c_2 are constants

By squaring Equation (A.2), we obtain

$$S_{wi}^2 = b^2\Phi^{-2c_2}.$$ (A.3)

By multiplying Equation (A.1) by (A.3), we obtain the following equations:

$$|\ln(k)| \times S_{wi}^2 = a\Phi^{c_1} \times b^2\Phi^{-2c_2},$$ (A.4)

$$\frac{|\ln(k)| \times S_{wi}^2}{\Phi^{c_1} \times \Phi^{-2c_2}} = ab^2,$$ (A.5)

$$\frac{|\ln(k)| \times S_{wi}^2}{\Phi^{c_1-2c_2}} = ab^2,$$ (A.6)

$$\frac{|\ln(k)|}{\Phi^{c_1-2c_2}} \times S_{wi}^2 = b^2.$$ (A.7)

By taking a square root of Equation (A.7), we obtain

$$\sqrt{\frac{|\ln(k)|}{\Phi^{c_1-2c_2}}} \times S_{wi} = \sqrt{ab^2}.$$ (A.8)

By replacing $\sqrt{ab^2}$ with Cn, we have

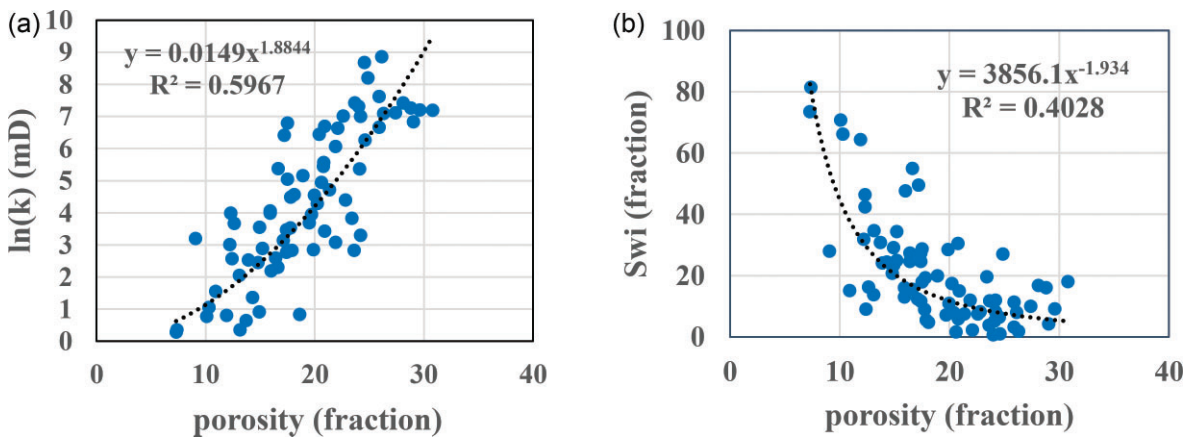$$\sqrt{\frac{|\ln(k)|}{\Phi^{c_1-2c_2}}} \times S_{wi} = Cn.$$ (A.9)

Figure A.1. (a) plot of $|\ln(k)|$ vs Φ, (b) plot of S_{wi} vs Φ.
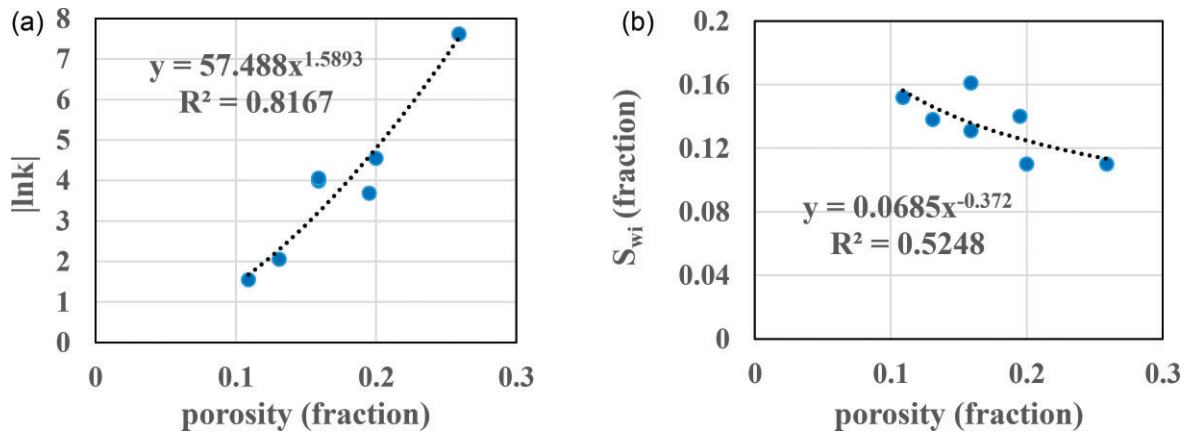

Figure A.2. (a) plot of $|\ln k|$ vs Φ for CRT-2, (b) plot of S_{wi} vs Φ for CRT-2.

Equation (A.9) is transformed to equation (13) when $c_1 -_2 c_2$ is equal to one. The reason why the value of $c_1 -_2 c_2$ deviates from one is that the experimental data are scattered (see Section 3.2 and figure 2e). We chose the best trend to fit the experimental data in figure A.1a and b, which has the maximum R^2 and fits reality better. However, several trends may be fitted to the experimental data and several equations may be obtained. Therefore, equation (13) is not the only equation. Note that this is a limitation to the solid proof of equation (13).

Figure A.2 parts a and b for CRT-2 are created to describe a case study using the data from Table 1. As shown in figure A.2a, $C_1 = 1.59$ and $a = 57.5$, and from figure A.2b, $C_2 = 0.37$ and $b = 0.07$. Calculating $c_1 -_2 c_2$ gives $1.59 - (2 \times 0.37) = 0.85$, which is close to 1. The deviation from 1 could be caused by scattering of the data. $C_2 = 0.53$ is calculated from $a = 57.5$ and $b = 0.07$, $(C_2 = \sqrt{ab^2})$. C_2 is chosen between 0.4 and 0.8 for CRT-2 (see Table 3). As shown, the value of $C_2 = 0.53$ is between 0.4 and 0.8, $(0.4 < 0.53 < 0.8)$. Moreover, the arithmetic mean of the lower and upper bounds of C2 for CRT-2 is 0.6, which is close to 0.53.

References

Aguilera, R., 2002. Incorporating capillary pressure, pore throat aperture radii, height above free-water table, and Winland r 35 values on Pickett plots, *AAPG Culletin*, **86**, 605–624.

Amaefule, J.O., Altunbay, M., Tiab, D., Kersey, D.G. & Keelan, D.K., 1993. Enhanced reservoir description: using core and log data to identify hydraulic (flow) units and predict permeability in uncored intervals/wells, in *SPE Annual Technical Conference and Exhibition*. OnePetro.

Amyx, J.W., Bass, D.M. & Whiting, R.L., 1960. *Petroleum Reservoir Engineering: Physical Properties*. McGraw-Hill College.

Balan, B., Mohaghegh, S. & Ameri, S., 1995. State-of-the-art in permeability determination from well log data: part 1—a comparative study, model development, in *SPE Eastern Regional Conference and Exhibition*, https://doi.org/10.2118/30978-ms.

Bordenave, M.L. & Hegre, J.A., 2005. The influence of tectonics on the entrapment of oil in the Dezful Embayment, Zagros Foldbelt, Iran, *Journal of Petroleum Geology*, **28**, 339–368.

Carman, P.C., 1937. Fluid flow through granular beds. AIChE, **15**, 150–156..

Coates, G. & Denoo, S., 1981. The producibility answer product, *The Technical Review*, **29**, 54–63.

Dakhelpour-Ghoveifel, J., Shegeftfard, M. & Dejam, M., 2019. Capillary-based method for rock typing in transition zone of carbonate reservoirs, *Journal of Petroleum Exploration and Production Technology*, **9**, 2009–2018.

Ghadami, N., Rasaei, M.R., Hejri, S., Sajedian, A. & Afsari, K., 2015. Consistent porosity–permeability modeling, reservoir rock typing and hydraulic flow unitization in a giant carbonate reservoir, *Journal of Petroleum Science & Engineering*, **131**, 58–69.

Gunter, G.W., Finneran, J.M., Hartmann, D.J. & Miller, J.D., 1997. Early determination of reservoir flow units using an integrated petrophysical method, in *SPE Annual Technical Conference and Exhibition.* OnePetro.

Guo, G., Diaz, M.A., Paz, F., Smalley, J. & Waninger, E.A., 2007. Rock typing as an effective tool for permeability and water-saturation modeling: a case study in a clastic reservoir in the Oriente Basin, *SPE Reservoir Evaluation & Engineering*, **10**, 730–739.

Haidari, K., Amini, A., Aleali, M. & Solgi, A., 2020. Distribution pattern of Ahwaz sandstone and Kalhur evaporite members of Asmari Formation in Dezful Embayment and Abadan plain, a basis for stratigraphic traps studies, *Geopersia*, **10**, 53–63.

Izadi, M. & Ghalambor, A., 2013. A new approach in permeability and hydraulic-flow-unit determination, *SPE Reservoir Evaluation & Engineering*, **16**, 257–264.

Kelkar, M. & Perez, G., 2002. Applied geostatistics for reservoir characterization, in *Applied Geostatistics for Reservoir Characterization*, https://doi.org/10.2118/9781555630959.

Kolodzie, S., 1980. Analysis of pore throat size and use of the Waxman-Smits equation to determine OOIP in Spindle Field, Colorado, in *SPE Annual Technical Conference and Exhibition*, https://doi.org/10.2118/9382-ms.

Kozeny, J., 1927. Uber kapillare Leitung des Wassers im Boden-Aufstieg, Versickerung und Anwendung auf die Bewasserung, Sitzungsberichte der Akademie der Wissenschaften Wien, *Mathematisch Naturwissenschaftliche Abteilung*, **136**, 271–306.

Lalanne, B. & Rebelle, M., 2014. A review of alternative methods to classify rock-types from capillary pressure measurements, in *IPTC 2014: International Petroleum Technology Conference*, https://doi.org/10.2523/iptc-17631-ms.

Leverett, M., 1941. Capillary behavior in porous solids, *Transactions of the AIME*, **142**, 152–169.

Mirzaei-Paiaman, A., Saboorian-Jooybari, H., Chen, Z. & Ostadhassan, M., 2019b. New technique of true effective mobility (TEM-Function) in dynamic rock typing: reduction of uncertainties in relative permeability data for reservoir simulation, *Journal of Petroleum Science and Engineering*, **179**, 210–227.

Mirzaei-Paiaman, A., Saboorian-Jooybari, H. & Pourafshary, P., 2015. Improved method to identify hydraulic flow units for reservoir characterization, *Energy Technology*, **3**, 726–733.

Moradi, M., Moussavi-Harami, R., Mahboubi, A., Khanehbad, M. & Ghabeishavi, A., 2017. Rock typing using geological and petrophysical data in the Asmari reservoir, Aghajari Oilfield, SW Iran, *Journal of Petroleum Science and Engineering*, **152**, 523–537.

Morris, R.L. & Biggs, W.P., 1967. Using log-derived values of water saturation and porosity, In *SPWLA 8th Annual Logging Symposium.* OnePetro.

Nabawy, B.S. & El Sharawy, M.S., 2015. Hydrocarbon potential, structural setting and depositional environments of Hammam Faraun Member of the Belayim Formation, Southern Gulf of Suez, Egypt, *Journal of African Earth Sciences*, **112**, 93–110.

Nooruddin, H.A. & Hossain, M.E., 2011. Modified Kozeny–Carmen correlation for enhanced hydraulic flow unit characterization, *Journal of Petroleum Science and Engineering*, **80**, 107–115.

Opera, A., Alizadeh, B., Sarafdokht, H., Janbaz, M., Fouladvand, R. & Heidarifard, M.H., 2013. Burial history reconstruction and thermal maturity modeling for the Middle Cretaceous–Early Miocene Petroleum System, southern Dezful Embayment, SW Iran, *International Journal of Coal Geology*, **120**, 1–14.

Pittman, E.D., 1992. Relationship of porosity and permeability to various parameters derived from mercury injection-capillary pressure curves for sandstone, *AAPG Bulletin*, **76.2**, 191–198.

Rabbani, A.R. & Bagheri Tirtashi, R., 2010. Hydrocarbon source rock evaluation of the super giant Ahwaz oil field, SW Iran, *Australian Journal of Basic and Applied Sciences*, **4**, 673–686.

Rahimpour-Bonab, H., Mehrabi, H., Navidtalab, A. & Izadi-Mazidi, E., 2012. Flow unit distribution and reservoir modelling in cretaceous carbonates of the Sarvak Formation, Abteymour Oilfield, Dezful Embayment, SW Iran, *Journal of Petroleum Geology*, **35**, 213–236.

Riazi, Z., 2018. Application of integrated rock typing and flow units identification methods for an Iranian carbonate reservoir, *Journal of Petroleum Science and Engineering*, **160**, 483–497.

Saner, S., Kissami, M. & Nufaili, S.A., 1997. Estimation of permeability from well logs using resistivity and saturation data, *SPE Formation Evaluation*, **12**, 27–31.

Shabaninejad, M. & Bagheripour Haghighi, M., 2011. Rock typing and generalization of permeability-porosity relationship for an Iranian carbonate gas reservoir, in *SPE Nigeria Annual International Conference and Exhibition*, https://doi.org/10.2118/150819-ms.

Shedid, S.A. & Almehaideb, R.A., 2002. A new approach of reservoir description of carbonate reservoirs, in *SPE International Petroleum Conference and Exhibition in Mexico*, https://doi.org/10.2523/74344-ms.

Shenawi, S.H., White, J.P., Elrafie, E.A. & Kilany, K.A., 2007. Permeability and water saturation distribution by lithologic facies and hydraulic units: a reservoir simulation case study, in *SPE Middle East Oil and Gas Show and Conference*, https://doi.org/10.2118/105273-ms.

Siddiqui, S., Okasha, T.M., Funk, J.J. & Al-Harbi, A.M., 2003. SCA2003-40: new representative sample selection criteria for special core analysis, in *Symposium A Quarterly Journal In Modern Foreign Literatures*.

Siddiqui, S., Okasha, T.M., Funk, J.J. & Al-Harbi, A.M., 2006. Improvements in the selection criteria for the representative special core analysis samples, *SPE Reservoir Evaluation & Engineering*, **9**, 647–653.

Soleimani, B., Moradi, M. & Ghabeishavi, A., 2018. Stoneley wave predicted permeability and electrofacies correlation in the Bangestan Reservoir, Mansouri Oilfield, SW Iran, *Geofísica Internacional*, **57**, 107–120.

Soleymanzadeh, A., Jamialahmadi, M., Helalizadeh, A. & Soulgani, B.S., 2018. A new technique for electrical rock typing and estimation of cementation factor in carbonate rocks, *Journal of Petroleum Science and Engineering*, **166**, 381–388.

Soleymanzadeh, A., Parvin, S. & Kord, S., 2019. Effect of overburden pressure on determination of reservoir rock types using RQI/FZI, FZI* and Winland methods in carbonate rocks, *Petroleum Science*, **16**, 1403–1416.

Speight, J.G., 2014. *Handbook of Offshore Oil and Gas Operations*, Elsevier, https://doi.org/10.1016/C2009-0-19144-4.

Timur, A., 1968. An investigation of permeability, porosity, and residual water saturation relationships, in *SPWLA 9th Annual Logging Symposium.* OnePetro.

Willhite, G.P., 1986. Waterflooding, in *Waterflooding*, https://doi.org/10.2118/9781555630058.

Winland, H.D., 1972. Oil accumulation in response to pore size changes, Weyburn field, Saskatchewan, Amoco Production Company report F72-G-25 (unpublished), Tulsa, OK, 20.

Ye, S., Lü, Z. & Li, R., 2011. Petrophysical and capillary pressure properties of the upper Triassic Xujiahe Formation tight gas sandstones in western Sichuan, *China. Petroleum Science*, **8**, 34–42.